Hidden-sector photon and axion searches using photonic band gap structures

2014 J. Phys. G: Nucl. Part. Phys. 41 035005

(http://iopscience.iop.org/0954-3899/41/3/035005)

OPEN ACCESS
IOP Publishing
Journal of Physics G: Nuclear and Particle Physics
J. Phys. G: Nucl. Part. Phys. **41** (2014) 035005 (10pp)
doi:10.1088/0954-3899/41/3/035005

Hidden-sector photon and axion searches using photonic band gap structures

Rebecca Seviour[1,2], **Ian Bailey**[3,4], **Nathan Woollett**[3,4] **and Peter Williams**[4,5]

[1] University of Huddersfield, Huddersfield, UK
[2] Lund University, Lund, Sweden
[3] Physics Department, Lancaster University, Lancaster, UK
[4] Cockcroft Institute, Sci-Tech Daresbury, Warrington, Cheshire, UK
[5] STFC Daresbury Laboratory, Sci-Tech Daresbury, Warrington, Cheshire, UK

E-mail: i.bailey@lancaster.ac.uk

Received 5 August 2013, revised 20 December 2013
Accepted for publication 6 January 2014
Published 12 February 2014

Abstract
Many proposed extensions of the standard model of particle physics predict the existence of weakly interacting sub-eV particles (WISPs) such as hidden-sector photons and axions, which are also of interest as dark matter candidates. In this paper we propose a novel experimental approach in which microwave photonic lattice structures form part of a 'light shining through the wall'-type experiment to search for WISPs. We demonstrate the potential to match and exceed the sensitivities of conventional experiments operating in the microwave regime.

Keywords: axions, hidden-sector photons, microwave photonics

(Some figures may appear in colour only in the online journal)

1. Introduction

Among the weakly interacting sub-eV particles (WISPs) hypothesized to exist are additional gauge bosons such as hidden-sector photons (HSPs) and pseudo-Goldstone bosons such as axions. These light bosons are predicted to give rise to a range of observable effects [1]; for example, an axion with a mass in the range $10^{-6} < m_A < 10^{-2}$ eV would be an ideal candidate to explain cold dark matter observations [2]. Note that in this paper 'axions' is used to refer to both Peccei–Quinn axions and generic axion-like scalar particles. Currently, a variety of astrophysical arguments and laboratory experiments indicate that the axion mass should be

lower than 10^{-2} eV [3], a mass range over which the parameters of HSPs are also relatively unconstrained by experiment. In this paper we propose a novel experimental technique to detect WISPs with masses in the range $10^{-4.5} < m < 10^{-3.5}$ eV.

Axion searches endeavour to detect the conversion between a photon and an axion in the presence of a static magnetic field via the Primakoff effect. Examples include astrophysical observations in helioscopes, such as the CERN axion solar telescope (CAST) which uses an LHC dipole magnet mounted with its primary axis directed toward the sun [4], and cavity searches for axions with galactic origins, such as the axion dark matter experiment (ADMX) [5]. A disadvantage of these approaches is that there is no direct control of the axion (or other WISP) source. In the case of helioscope searches, the production conditions are generally well-understood, and the limits obtained are only weakened in the case of specific temperature-dependent or density-dependent WISP models. More significantly, limits from galactic searches rely on assumptions regarding the local density of dark matter.

Alternatively, 'light shining through wall' (LSW) laser experiments [6, 7] use purely laboratory-based methods, free from external models. In these experiments intense infrared/visible radiation impinges on a wall, on the other side of which is a sensitive photon detector. To maximize the conversion probability, strong magnetic fields and intense radiation sources are required [8–10].

Unlike axions, massive HSPs would couple to standard model (SM) photons via kinetic mixing, resulting in vacuum oscillation between them, similar to flavour-changing neutrino oscillations. Current constraints on the associated coupling constant come from Cavendish-type tests of Coulomb's Law in the μeV to meV mass range [11, 12]. Sub-μeV constraints arise from the non-observation of distortions in the cosmic microwave background that would be produced by resonant production of HSPs [13]. In the few meV range model-independent bounds are being set by optical laser and intense accelerator-based free electron laser LSW experiments [8, 14, 15] but these have recently been surpassed by solar lifetime calculations [16, 17] which dominate the meV to keV range, including the region previously excluded by non-observation of photon regeneration in CAST [4].

To date none of these approaches has revealed evidence for the existence of WISPs, although they have been used to significantly constrain the allowed parameter spaces for both axion and HSP models. One direction for future experimental searches comes from Jaeckel and Ringwald [18] who propose realizing the LSW technique at RF frequencies with microwave cavities. This allows the theoretically interesting μeV mass range to be investigated with potentially four orders of magnitude greater sensitivity than other approaches. The primary reason for this vast improvement is the high quality factor (Q) of RF cavities [19–22]. At microwave frequencies standard copper cavities and superconducting cavities have Qs of order 10^3 and of order 10^9 respectively.

In the following sections we propose to extend the regime of WISP searches using photonic band gap (PBG) structures at microwave frequencies as an analogue to the LSW experiments of [6, 7] and to the proposals of Jaeckel and Ringwald. We concentrate on demonstrating the potential of this approach for HSPs as this allows for a simpler experimental design. However, as PBG structures do not require to be superconducting to achieve high Qs, a strong magnetic field could be applied to enable the same technique to be sensitive to axions.

The key parameters to be determined by any HSP search are the mass of the HSP m_γ and the probability that a HSP will convert to a photon, which is proportional to the square of the hidden sector mixing parameter χ. These parameters are referred to in the remainder of this paper and can best be understood by reference to the Lagrangian density [18]

$$\mathcal{L} = -\frac{1}{4}F^{\mu\nu}F_{\mu\nu} - \frac{1}{4}B^{\mu\nu}B_{\mu\nu} - \frac{\chi}{2}F^{\mu\nu}B_{\mu\nu} + \frac{m_\gamma^2}{2}B^{\mu}B_{\mu} \tag{1}$$

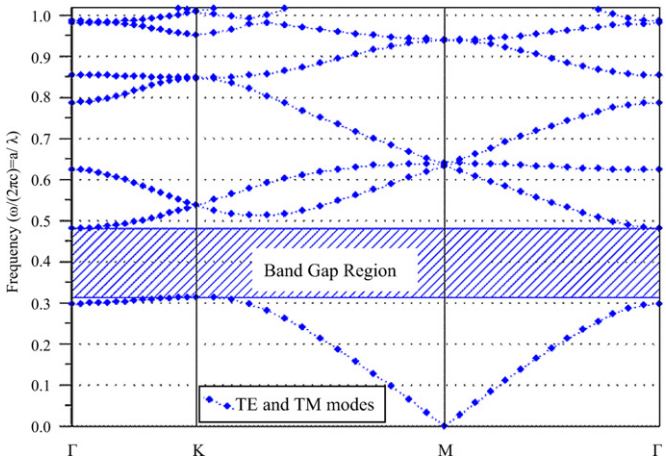

Figure 1. Band gap diagram of a sapphire-in-air, triangular lattice calculated using the commercial software package RSOFT [33].

where $F^{\mu\nu}$ is the usual electromagnetic field tensor and $B^{\mu\nu}$ is the equivalent hidden sector field tensor with associated gauge field B^{μ}.

2. Photonic structure

2.1. General properties

A PBG structure is a periodic array of varying permittivities forming a lattice of scatterers of EM radiation. PBGs have been extensively studied and have demonstrated a range of novel physical phenomena [23] leading to many applications [23, 24], particularly in lasing where defects in the lattice are used to produce highly-intense coherent radiation [24].

For certain lattice configurations, EM waves with specific frequencies are not able to propagate through the lattice. Figure 1 shows the band structure (wavenumber versus frequency) for a triangular 2D lattice of sapphire rods with the frequency normalized to the speed of light. A 'band gap' in propagating frequencies is clearly present.

It follows that PBG structures containing a defect in the periodic lattice can behave analogously to a conventional microwave resonant cavity. Wave propagation in this periodic structure is governed by Bloch–Floquet theory [23]. If an EM wave has a half-wavelength comparable to the size of the defect region and a frequency that lies inside the band gap, the 'mode' becomes spatially localized at the defect site [23]. The frequency dependence of the localization effect makes it possible to create a structure where a specific mode is confined, but all other modes propagate away from the defect site through the PBG lattice. The ability of the lattice to confine an EM field by virtue of the periodicity of the lattice alone, means the structure can confine EM modes to the defect regions without the need for any external waveguide or cavity to support the mode.

To define the EM field tensor in equation (1) and hence the range of χ which is measurable, we consider a specific PBG geometry consisting of a two-dimensional triangular lattice of sapphire scatterers with relative permittivity of 9.0 and filling factor 0.183, in a vacuum. These parameters define the propagation of EM waves in the photonic structure, the frequency and size of the band gap, and the frequency/Q of the confined EM state [25]. The choice of

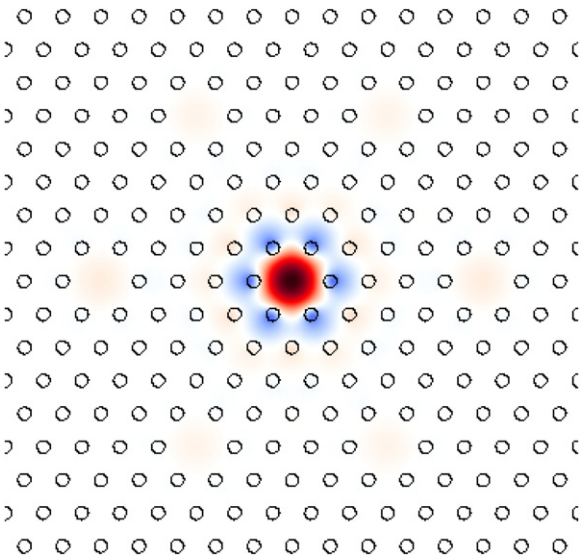

Figure 2. Multi-defect triangular lattice of scatterers showing the electric field distribution of a highly spatially-localized TM010 wave, generated using MEEP.

materials is determined by the thermal and mechanical properties, the frequency stability of the permittivity, and the permittivity contrast between the materials. In this case, sapphire is chosen as the authors of [26] have demonstrated that microwave sapphire PBG structures of the form discussed here can operate at powers over 2 MW if required, and the high permittivity contrast creates a well-defined band gap ideal for the experiment we propose.

The lattice parameters (and hence the filling factor) were determined using the numerical EM solver MEEP [27] to ensure that each defect in the lattice supports a narrow bandwidth EM state inside the band gap of the lattice. Using the technique presented in [27, 28] we have verified that Qs of 10^6–10^9 can be achieved using this type of lattice (comparable to those of SC cavities). In addition to potentially higher Qs, the use of PBG structures enables us to reach frequencies higher than those accessible to conventional microwave structures, thereby covering the regime from a few GHz to the infra-red. Typical lattice sizes are given later in section 2.3.

It is worth noting that as the lattice is formed from dielectric material, the application of a magnetic field through the lattice is straightforward, thereby enabling axion searches as well as HSP searches.

Figure 2 shows a simulation of the electric field distribution of a lattice with the described geometry, where defects have been created by the removal of scatterers so that there is a spatially-localized TM010 state in one of the defects. The natural symmetry presented by the lattice can be exploited to include multiple equivalent defects increasing the detector volume relative to a simple two-defect arrangement. In the configuration shown, the inner defect acts as an EM source (fed by an external source), and the outer defects act as detectors. For illustration, the detector defects have been placed close together so that they are clearly all coupled to the central defect. Conversely, if the detector defects are sufficiently distant that they are electrically decoupled from the source then any detected photons above the noise threshold represent transport mediated by non-SM processes. The requirements for achieving the necessary decoupling are explored in the next section.

2.2. Isolation of defects

In our lattice the defects are all identical, hence the EM field established in each defect is the split state of the single defect structure [29, 30]. This enables the use of a tight-binding model, with an analytical method based on the variational principle [31] extended to the case where the states in each defect become decoupled. Taking $\vec{E}_0(\vec{r})$ as the electric field at position $\vec{r}$ for a state associated with a single defect, $\vec{E}_0(\vec{r})$ obeys [23]:

$$\hat{H}\vec{E}_0(\vec{r}) = \left(\frac{\omega_0}{c}\right)^2 \epsilon(\vec{r})\vec{E}_0(\vec{r}), \tag{2}$$

where the operator $\hat{H}$ is defined as $\nabla \times \nabla \times$, ω_0 is the angular eigenfrequency, $\epsilon(\vec{r})$ the effective permittivity and c the speed of light. In the multi-defect case, each state is a superposition of each individual defect state [31]. For an m-defect structure with n resonant states we have,

$$\vec{E}_n(\vec{r}) = \sum_{i=1}^{m} C_{ni}\vec{E}_0(\vec{P}_i), \tag{3}$$

where $\vec{E}_n(\vec{r})$ is the nth state, $\vec{P}_i = \vec{r} - \vec{R}_i$, $\vec{R}_i$ is the coordinate of the ith defect and C_{ni} is the coefficient of the linear combination. Replacing the eigenfrequency ω_0 in equation (2) by the eigenfrequency of the nth eigenstate, ω_n shows that $\vec{E}_n(\vec{r})$ also satisfies equation (2). This forms a variational problem in which assigning different coefficients C_{ni} to each state creates different $\vec{E}_n(\vec{r})$. According to [23], the eigenvalue should correspond to the minimum of the variational equation,

$$\left(\frac{\omega_n}{c}\right)^2 = \min_{\vec{E}_n(\vec{r})} \frac{\int |\hat{H}\vec{E}_n(\vec{r})|^2 \,\mathrm{d}\vec{r}}{\int \epsilon(\vec{r})|\vec{E}_n(\vec{r})|^2 \,\mathrm{d}\vec{r}}$$

$$= \frac{\langle \vec{E}_n(\vec{r})|\hat{H}|\vec{E}_n(\vec{r})\rangle}{\langle \vec{E}_n(\vec{r})|\epsilon(\vec{r})|\vec{E}_n(\vec{r})\rangle} \tag{4}$$

$$= \frac{\sum_{ij} C_{ni}C_{nj}\mathbf{H}_{ij}}{\sum_{ij} C_{ni}C_{nj}\mathbf{S}_{ij}} \tag{5}$$

where

$$\mathbf{H}_{ij} = \langle \vec{E}_0(\vec{P}_i)|\hat{H}|\vec{E}_0(\vec{P}_j)\rangle,$$
$$\mathbf{S}_{ij} = \langle \vec{E}_0(\vec{P}_i)|\epsilon(\vec{r})|\vec{E}_0(\vec{P}_j)\rangle,$$

$\mathbf{H}_{ij}$ denotes the elements of the Hamiltonian, $\mathbf{S}_{ij}$ denotes the elements of the overlap matrix, i and j denote states localized on the ith and jth defects respectively. To simplify calculations, the eigenstate in the single-defect system $\vec{E}_0(\vec{r})$ is taken to be real and is normalized such that

$$\langle \vec{E}_0(\vec{r})|\epsilon(\vec{r})|\vec{E}_0(\vec{r})\rangle = \int \vec{E}_0(\vec{r})\epsilon(\vec{r})\vec{E}_0(\vec{r}) \,\mathrm{d}\vec{r} = 1. \tag{6}$$

Using this normalization, the values of $\mathbf{H}_{ij}$ for the seven-defect PC shown in figure 2 can be estimated as,

$$\mathbf{H}_{ij} = \begin{cases} (\omega_0/c)^2 & (i = j), \\ (\omega_0/c)^2\beta_{ij} & (i \neq j), \end{cases} \tag{7}$$

where $\beta_{ij} = \langle \vec{E}_0(\vec{P}_i)|\epsilon(\vec{P}_j)|\vec{E}_0(\vec{P}_j)\rangle$ describes the coupling strength between defects, and different β_{ij} are related to each other by the lattice symmetry. Here we assume that for an effective hidden sector search, each defect state must be spatially localized to that defect [31],

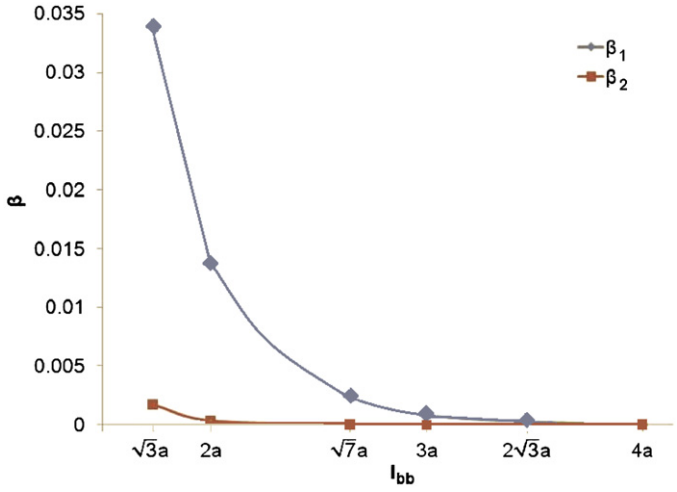

Figure 3. The dependence of the defect coupling coefficients β_i on the defect separation I_{bb} in units of the lattice constant 'a'. β_1 represents coupling between nearest neighbours and β_2 represents coupling between next-to-nearest neighbours.

such that it decouples from all other defects. This is achieved when the overlap term $\mathbf{S}_{ij}$ in equation (4) tends to zero for all $i \neq j$ such that,

$$\mathbf{S}_{ij} = \langle \vec{E}_0(\vec{P}_i)|\epsilon(\vec{r})|\vec{E}_0(\vec{P}_j)\rangle \approx \delta_{ij}. \tag{8}$$

The coefficients C_{ni} should be restricted to minimize the variational problem in equation (4) with the condition that C_{ni} gives stationary values, resulting in,

$$\det\left[\mathbf{H}_{ij} - \left(\frac{\omega_n}{c}\right)^2 \delta_{ij}\right] = 0. \tag{9}$$

This indicates that the allowed frequencies in a coupled-defect photonic lattice, ω_n, can be determined from the single-defect resonant frequency, ω_0 and the coupling coefficient β_{ij}.

Solving equation (8) using the least-squares method [31] enables us to study the dependence of the β_{ij} on the lattice properties. In the case of our example structure, the six-fold symmetry means that there are only three possible values of the coupling coefficient, corresponding to the coupling between nearest neighbours (β_1), next-to-nearest neighbours (β_2) and next-to-next-to-nearest neighbours (β_3). Figure 3 shows the dependence of both the nearest neighbour and next-to-nearest neighbour couplings on the separation between defects I_{bb} in the lattice. Coupling coefficients of order 10^{-24} were obtained when the separation between defects was 16 lattice constants. This semi-analytical study also acts to benchmark the more-detailed numeric simulations described below.

To verify that the source and detector defects are sufficiently decoupled, suppressing all SM transport of photons, MEEP simulations of the EM field were performed. The natural symmetry of the lattice was used to reduce the simulation domain to a two-defect sub-domain of figure 2. An excitation at the decoupled frequency ω_0 was simulated in the source defect and operated for approximately 40 RF cycles. Frequencies outside the band gap were allowed to disperse over a duration of 4200 RF cycles and then the EM field across the lattice and the detector defect was monitored for a further 120 RF cycles, where the latter is a small part of the data-taking period of the envisaged experiment. A representative example of the results is presented in figure 4 which shows suppression of the electric field strength in the detector defect by a factor of 10^5 relative to the field in the source region for a defect separation of 13

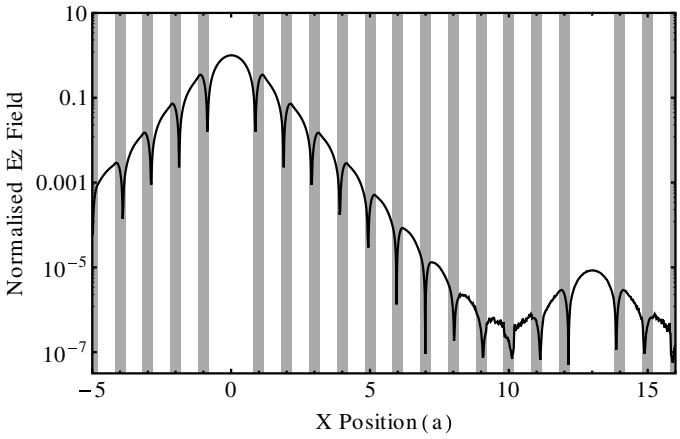

Figure 4. The normalized electric field along the central line between the source and detector. The position of the dielectric scatterers is indicated by the grey lines.

lattice constants. At 16 lattice spacings the suppression factor increases to 10^7, and at greater separations the simulations are limited by numerical noise.

The results from both the semi-analytical and full numeric simulations suggest that separations of 16 lattice spacings are sufficient to make the frequency shift due to coupling between detector defects negligible compared to the natural frequency width of the states localized in the defects. However, for maximum sensitivity, the coupling between the source and detector defects should be small enough that the dominant background in the detector defect is thermal noise. At liquid nitrogen temperatures, this requires that the power coupled into the detector defect through the lattice should be less that 10^{-24} W assuming a 1 mHz frequency resolution for the detector electronics. For a 1 kW source we therefore require a factor 10^{27} (260 dB) of suppression. Extrapolating from the MEEP simulations this requires a minimum of 30 lattice spacings, which is the number used in the remainder of this paper to determine the sensitivity of such structures to the presence of HSPs.

2.3. HSP sensitivity

Any photons mediated by HSPs between the source and detector defects in our structure would produce an excess above the thermal noise background. The probability of transmission of photons via the hidden sector is determined by the Q factors and by the geometric factor G [32],

$$G(k/\omega_0) \equiv \omega_0^2 \int_{v'} \int_{v} \mathrm{d}^3x\, \mathrm{d}^3y \frac{\exp(\mathrm{i}k|x-y|)}{4\pi|x-y|} A_{\omega 0}(y) A'_{\omega 0}(x), \tag{10}$$

where x and y are the co-ordinate systems centred on the source and detector regions respectively, A_{ω_0} and $A_{\omega 0'}$ are the (electric) field vectors of the source and detector states and k/ω_0 is a measure of the velocity of the HSP in the rest frame of the lattice. Figure 5 shows a plot of the G factor for the PBG structure used in figure 2 as a function of defect separation, where we take the optimal case of resonant HSP production corresponding to k/ω_0 being close to zero. As can be seen, for the types of lattices we consider in our paper where defect regions are separated by 30 lattice constants (as required from the studies highlighted in section 2.2) the value of G is approximately 0.001.

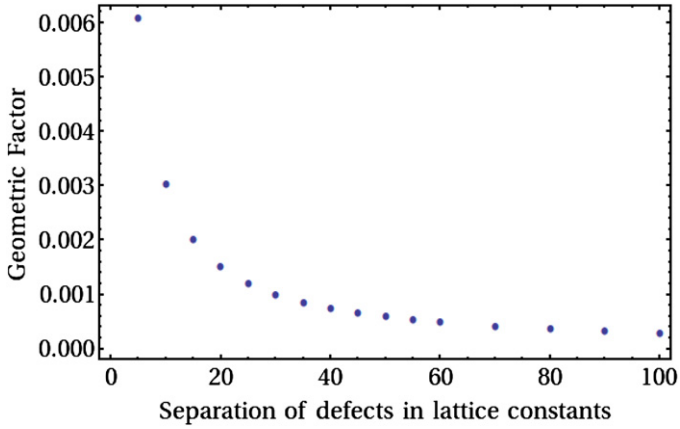

Figure 5. Maximum G factor between a source and defect region for the PBG structure used in figure 2 as a function of separation between the source and defect.

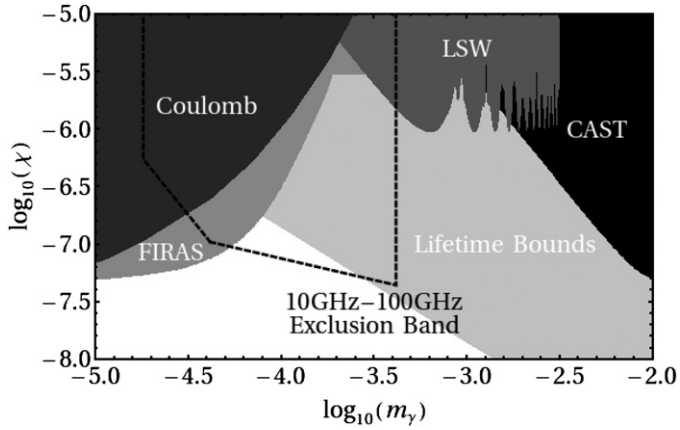

Figure 6. Current bounds on hidden-sector photons from some of the different experiments discussed at the beginning of the paper. The dashed line indicates the potential bounds of the PBG proposed experiment calculated in this paper corresponding to a range of lattices parameters of the order of millimetres.

We have analysed the EM field distribution of the PBG structure to determine the χ exclusion sensitivity for a given m_γ, where we can relate m_γ of the HSP to the frequency of excitation of the source. Assuming that the seven-defect structure is cooled to liquid nitrogen temperatures, each defect is separated by 30 lattice spacings and 1 kW of power is supplied to the central defect via a coaxial waveguide we obtain an estimated exclusion which is shown by the dashed curve in figure 6. The curve corresponds to the expected 3σ exclusion with approximately 1 year of running, or equivalently to the expected 5σ exclusion with less than 3 years of running. The operating parameters used have been deliberately chosen to be conservative.

The bounds on the range of operation of the PBG structure for HSPs from figure 6 enable us to specify the parameters of the lattice. Although detailed analysis needs to be undertaken for a specific geometry we can estimate to an accuracy of 1% the dimensions required for our proposed structure. At 10 GHz our sapphire scatterers would have a radius of 2 mm and a

separation of 9 mm, and at 100 GHz our sapphire scatterers would have a radius of 200 μm and a separation of 0.9 mm. The lattice would be 80 by 80 scatterers in size, surrounded by microwave absorbent material (to ensure no outside interference). This configuration, and the method for coupling the EM field into the lattice and out of the lattice is the same as that presented in [25].

3. Summary

In this paper we have demonstrated that a compact multi-defect photonic lattice can create very high Q resonators in which nearby defects can be decoupled from each other, providing an environment where transport mediated by non-SM processes can be measured. In addition, by including a large number of defects the probability of a photon produced from an axion or hidden-sector photon (HSP) exciting a defect region can be increased to maximise the sensitivity of an experiment. As shown by figure 6, PBG structures are a promising technology for LSW-type experiments and should be able to make a substantial contribution to model-independent HSP searches.

We intend to realise the 2D structures proposed in this paper by constructing a multi-layered heterostructure of dielectric materials, where our seven-defect lattice will be sandwiched between two defect-free lattices to create a pseudo-two-dimensional structure.

Suitable PBG structures can be formed from dielectric materials in air/vacuum, and unlike conventional microwave resonators an external magnetic field may be applied over the defect resonator region. Using an external EM source to excite a resonant state in a central defect, the defects surrounding the central resonator will act as our detectors for couplings mediated by non-SM processes, while any photons will be confined by the high Q factor of the defects. Detection of excited states will be accomplished using a spectrum analyser connected to antennas placed in the vicinity of the defects, using the approach outlined in [25]. This will enable us to examine parts of the HSP parameter space beyond the scope of current experiments in the GHz to infra-red regime.

Acknowledgments

This research was funded in part by the EOARD grant FA8655-13-1-2111 and the STFC Cockcroft Institute Core grant no. ST/G008248/1.

References

[1] Jaeckel J and Ringwald A 2010 *Ann. Rev. Nucl. Part. Sci.* **60** 405
[2] Sikivie P 2011 *Phys. Lett.* B **695** 22
[3] Beringer *et al* (Particle Data Group) 2012 *Phys. Rev.* D **86** 010001
[4] Andriamonje S *et al* 2007 *J. Cosmol. Astropart. Phys.* JCAP04(2007)010
[5] Asztalos S J *et al* 2010 *Phys. Rev. Lett.* **104** 041301
[6] Hoogeveen F and Ziegenhagen T 1991 *Nucl. Phys.* B **358** 3
[7] Sikivie P, Tanner D B and van Bibber K 2007 *Phys. Rev. Lett.* **98** 172002
[8] Ruoso G, Cameron R, Cantatore G, Melissinos A C, Semertzidis Y, Halama H, Lazarus D and Prodell A 1992 *Z. Phys.* C **56** 505
[9] Afanasev A, Baker O K, Beard K B, Biallas G, Boyce J, Minarni M, Ramdon R, Shinn M and Slocum P 2008 *Phys. Rev. Lett.* **101** 120401
[10] Chou A S, Wester W, Baumbaugh A, Gustafson H R, Irizarry-Valle Y, Mazur P O, Steffen J H, Tomlin R, Yang X and Yoo J 2008 *Phys. Rev. Lett.* **100** 080402
[11] Williams E R, Faller J E and Hill H A 1971 *Phys. Rev. Lett.* **26** 721–4
[12] Bartlett D F and Loegl S 1988 *Phys. Rev. Lett.* **61** 2285–7

[13] Jaeckel J, Redondo J and Ringwald A 2008 *Phys. Rev. Lett.* **101** 131801
[14] Robilliard C, Battesti R, Fouché M, Mauchain J, Sautivet A-M, Amiranoff F and Rizzo C 2007 *Phys. Rev. Lett.* **99** 190403
[15] Ehret K *et al* 2010 *Phys. Lett.*B **689** 149–55
[16] Haipeng A, Pospelov M and Pradler J 2013 *Phys. Lett.* B **725** 190–5
[17] Haipeng A, Pospelov M and Pradler J 2013 *Phys. Rev. Lett.* **111** 041302
[18] Jaeckel J and Ringwald A 2008 *Phys. Lett.*B **659** 509–14
[19] Slocum P L, Baker O K, Hirshfield J L, Jiang Y, Kazakevitch G, Kazakov S, LaPointe M A, Martin A, Shchelkunov S and Szymkowiak A 2010 *Proc. Patras Workshop on Axions, WIMPs and WISPs* p 49
[20] Betz M and Caspers F 2012 *Proc. IPAC'12 (New Orleans)* THPPC021
[21] Povey R, Hartnett J and Tobar M 2010 *Phys. Rev.* D **82** 052003
[22] Williams P H 2010 *Proc. Patras Workshop on Axions, WIMPs and WISPs* p 37
[23] Joannopoulos J D, Johnson S G, Winn J N and Meade R D 2008 *Photonic Crystals: Molding the Flow of Light* (Princeton, NJ: Princeton University Press)
[24] Busch K, Lolkes S, Wehrspohn R B and Foll H 2004 *Photonic Crystals: Advances in Design, Fabrication and Characterization* (New York: Wiley)
[25] Xu Y and Seviour R 2012 *New J. Phys.* **14** 013014
[26] Munroe B, Cook A, Shapiro M and Temkin R 2012 *Proc. IPAC'12 (New Orleans)* TUPPR070
[27] Rodriguez A, Ibanescu M, Bermel P, Joannopoulos J D, Johnson S G, Farjadpour A, Roundy D and Burr G 2006 *Opt. Lett.* **31** 2972–83
[28] Joannopoulos J D, Rodriguez A, Ibanescu M and Johnson S G 2005 *Opt. Lett.* **30** 3192–5
[29] Temelkuran B, Bayindir M and Ozbay E 2000 *Phys. Rev. Lett.* **84** 2140–3
[30] Bulu I, Ozbay E, Bayindir M and Cubukcu E 2002 *IEEE J. Quantum Electron.* **38** 837–43
[31] Lin B-S 2003 *Phys. Rev.* E **68** 036611
[32] Jaeckel J, Massó E, Redondo J, Ringwald A and Takahashi F 2007 *Phys. Rev.* D **75** 013004
[33] Synopsys 2014 RSoft Fullwave FDTD code (http://optics.synopsys.com/rsoft)